communications earth & environment

Article

A Nature Portfolio journal

https://doi.org/10.1038/s43247-025-02145-z

Soil moisture-atmosphere interactions drive terrestrial carbon-water trade-offs

Wenqi Sun[1,2], Sha Zhou[1,2] ✉, Bofu Yu[3], Yao Zhang[4], Trevor Keenan[5,6] & Bojie Fu[7]

Soil moisture is coupled with vegetation and atmosphere, influencing global cycling of water, carbon, and energy. However, it remains unclear how soil moisture-atmosphere interactions affect land-atmosphere carbon and water exchanges simultaneously. Using Earth system model experiments, we show widespread carbon-water trade-offs between net ecosystem production and precipitation-minus-evapotranspiration driven by soil moisture dynamics. Soil moisture positively controls net ecosystem production and negatively affects precipitation-minus-evapotranspiration, through direct soil water stress and indirect soil moisture-atmosphere feedbacks. While soil moisture variability magnifies the interannual variability of net ecosystem production, it moderates that of precipitation-minus-evapotranspiration over land. These opposing effects lead to a pronounced carbon-water trade-off, which originates from the interplay between carbon acquisition through photosynthesis and water extraction through evapotranspiration. This trade-off is projected to intensify in a warming and drying future, as soil moisture increasingly regulates carbon and water exchanges, posing a serious challenge to sustaining both terrestrial carbon sink and water supply.

Climate change and rising atmospheric CO_2 concentration have altered terrestrial carbon and water cycles and will continue to impact terrestrial carbon uptake and water availability in the future[1–3]. Greater climate variability and more frequent climate extremes, such as heatwaves, droughts, and floods, would increase the inter-annual variability of carbon uptake and water availability, which pose great challenges to food and water security and the sustainability of ecosystem services[4–6]. In response to climate change and elevated CO_2, changes in soil moisture (SM) and vegetation cover further affect carbon and water fluxes at the land surface and consequently the atmosphere and climate[7,8]. While previous studies have demonstrated the crucial role of SM-atmosphere interactions in regulating terrestrial carbon or water cycling, especially over drylands[9–14], it remains unclear how the relationship between carbon uptake and water availability will be altered by SM changes in a CO_2-warmed world. Answers to this question are increasingly important as SM is projected to become more variable in space and time[15] and the coupling of carbon uptake and water availability is critical to achieving a number of Sustainable Development Goals (SDGs), e.g., climate change mitigation (SDG 13) and food and water security (SDG 2 and 6)[16,17]. In addition, it is largely unknown how SM-atmosphere interactions influence the long-term changes in terrestrial carbon uptake and water availability simultaneously, and the synergies and trade-offs between these ecosystem services in the future.

In water-limited ecosystems, SM dynamics directly determine the amount of water extracted by plant roots and plant water status, which in turn regulate stomatal conductance and the rate of photosynthetic carbon sequestration, i.e., gross primary production (GPP), and water loss via transpiration[18–20]. In addition, SM modifies soil evaporation and carbon loss through respiration (R), and hence exchanges of carbon and water fluxes, i.e., net ecosystem production (NEP) and evapotranspiration (E), between the land surface and the atmosphere[9,21]. As both NEP and E are positively controlled by soil water stress, these processes result in a delicate balance between carbon uptake and water loss under water-limited conditions[20,22]. On the other hand, SM is coupled with the atmosphere and indirectly influences carbon and water cycling through land-atmosphere feedbacks[7,23]. Reduced SM can shift latent cooling to sensible heating and accelerate atmospheric warming and drying, which further reduces NEP to a greater extent than the direct effect of soil water limitation[7,9,23,24]. SM can also affect precipitation (P) through moisture recycling and changes in mesoscale

[1]State Key Laboratory of Earth Surface Processes and Hazards Risk Governance (ESPHR), Faculty of Geographical Science, Beijing Normal University, Beijing, China. [2]Institute of Land Surface System and Sustainable Development, Faculty of Geographical Science, Beijing Normal University, Beijing, China. [3]School of Engineering and Built Environment, Griffith University, Nathan, QLD, Australia. [4]Institute of Carbon Neutrality, Sino-French Institute for Earth System Science, College of Urban and Environmental Sciences, Peking University, Beijing, China. [5]Department of Environmental Science, Policy and Management, University of California Berkeley, Berkeley, CA, USA. [6]Climate and Ecosystem Sciences Division, Lawrence Berkeley National Laboratory, Berkeley, CA, USA. [7]State Key Laboratory of Urban and Regional Ecology, Research Center for Eco-Environmental Sciences, Chinese Academy of Sciences, Beijing, China. ✉e-mail: shazhou21@bnu.edu.cn

circulations[25–27], but the indirect SM effect on P is weaker than the direct, positive effect of SM on E, resulting in a negative effect of SM on surface water availability (P-E), i.e., the amount of water available for runoff and water storage change, over most land areas[11,12].

Integrating the direct and indirect land-atmosphere processes, the overall influences of SM on NEP and P-E are opposite[7,9,11,12]. This suggests a likely trade-off between carbon uptake and water availability induced by SM–atmosphere interactions. While SM-induced carbon-water trade-off as a hypothesis has not been rigorously tested and evaluated, we expect this trade-off to be analogous to the well-recognized trade-off between carbon sink (or food production) and freshwater supply due to land use changes and vegetation greening[28–31], as SM stress can greatly limit vegetation growth and associated carbon sequestration and water loss, and in fact the effects of SM and vegetation on carbon and water fluxes are known to be strongly coupled within the soil-plant-atmosphere continuum[32,33]. To test this hypothesis, we investigate when and where the SM-induced trade-off between carbon uptake and water availability occurs and how this trade-off may change in a warmer and higher CO_2 future. This is crucial to our predictive capability of terrestrial carbon sink, food production, and freshwater availability, and our ability to manage terrestrial ecosystems for climate change mitigation and adaptation[34].

To assess the long-term SM effects on terrestrial carbon uptake and water availability and particularly the coupling of carbon and water cycling, we use three state-of-the-art Earth System Models (ESMs) that have participated in the Land Feedback Model Intercomparison Project (LFMIP)[35] and the historical and future (Shared Socioeconomic Pathway SSP5-8.5) simulations in the Coupled Model Intercomparison Project phase 6 (CMIP6)[36]. These experiments are driven by the same forcing agents except for the SM settings: SM is fully coupled with the atmosphere in historical and SSP5-8.5 simulations (Hist&SSP) and prescribed as the 1980–2014 climatology (pdLC) and a transient 30-year running mean climatology (rmLC) in the two experiments of LFMIP (Methods and Fig. S1). By comparing the three experiments, we can isolate the total SM effects (Hist&SSP minus pdLC), including the effects of SM trends (rmLC minus pdLC) and variability (Hist&SSP minus rmLC), on the mean and interannual variability of NEP and P-E, and test and evaluate the underlying trade-off between the two. To better understand the trade-off between NEP and P-E, we disentangle the relationship between SM-induced changes in carbon (GPP and R) and water (P and E) fluxes and evaluate their contributions to the coupling of NEP and P-E at the ecosystem scale. To identify whether and to what extent the model simulations could represent the real world, we also evaluate the effects of SM on NEP and P-E using observation-based datasets from the ERA5 global reanalysis[37] and FLUXCOM[38].

Results

Opposite SM effects on carbon uptake and water availability

It is clear from Fig. 1 that SM exerts opposite effects on NEP and P-E during the period of 1980–2099. Compared to pdLC, changes in SM reduce the global mean NEP by 0.60 Pg C $year^{-1}$ on average in Hist&SSP, and increase P-E by 15.1 mm $year^{-1}$ over the same 120-year period (Fig. 1a, b). SM variability alone reduces NEP by 0.26 Pg C $year^{-1}$, which accounts for 43% of the total SM effect, and a larger proportion of 57% can be attributed to the long-term SM trends (0.34 Pg C $year^{-1}$) (Fig. 1a). In contrast, SM variability increases P-E by 18.0 mm $year^{-1}$, which offsets the negative effect arising from the long-term SM trends (−2.9 mm $year^{-1}$), resulting in a net increase in P-E induced by SM changes (Fig. 1b).

The divergent SM effects on NEP and P-E are evident over many land areas (Fig. 1c-h). SM is projected to decrease in the Amazon and subtropical dry regions, resulting in a large decline in NEP and an increase in P-E during the study period (Fig. 1c, d, g and Fig. S2a, b). We also find that NEP increases and P-E decreases with the increase of SM in Central Africa (Fig. 1c, d, g and Fig. S2a, b). Considering the model spread in SM changes, we examine SM-induced changes in NEP and P-E in each ESM. The positive SM effect on NEP and the negative SM effect on P-E are evident for areas where SM decreases or increases (Fig. S3), which demonstrate the robustness of divergent SM effects on NEP and P-E. On the other hand, SM variability reduces NEP and increases P-E over many mid-latitude areas and at the global scale (Fig. 1a, b and Fig. S2c, d). This suggests non-linear impacts of SM on NEP and P-E, as decreases in NEP and increases in P-E under dry SM conditions are not compensated by increased NEP and decreased P-E under wet conditions[9,12].

Beyond the divergent impacts on the mean, we further show that SM variations substantially affect the inter-annual variability of NEP and P-E in an opposing manner (Fig. 1e, f, h). In tropical and subtropical regions where SM strongly influences the water fluxes, we find reduced variability in P-E induced by SM variability (Fig. 1f and Fig. S2h), partly because the negative SM feedback on P-E attenuates the magnitude and frequency of extreme P-E events[11,12]. However, SM variability enhances the interannual variability in NEP over almost all vegetated areas (Fig. 1e and Fig. S2g), which is consistent with previous findings that SM variability accounts for a large fraction of the interannual variability in carbon fluxes[7,39,40]. Together, these analyses provide modeling evidence of strong and opposite SM effects on the long-term mean and variability of net carbon and water fluxes and imply a crucial role that SM dynamics play in shaping a trade-off relationship between carbon uptake and water availability.

Spatial-temporal variation of the SM effects on carbon uptake and water availability

To test the robustness of the SM effects on carbon uptake and water availability, we assess the sensitivity of these fluxes to SM using Pearson and Spearman correlation coefficients based on observation-based datasets and model outputs from Hist&SSP (Methods and Figs. 2 and S4). The correlation analysis corroborates the findings of a positive effect of SM on NEP and a negative SM effect on P-E from the LFMIP experiments (Figs. 1 and 2). Moreover, models and observations consistently show that the SM effects on NEP and P-E vary spatially and seasonally, with significant signals in dry seasons over water-limited regions (Figs. 2 and S4).

Increased SM enhances NEP in dry regions/seasons but reduces NEP in wet regions/seasons (Fig. 2a-c, g-i). This is because terrestrial carbon uptake, particularly photosynthesis, is constrained by SM under water-limited conditions, but high SM can promote cloud formation and inhibit solar radiation for photosynthesis in a wet environment[9,23]. In addition, soil drying reduces evapotranspiration and evaporative cooling, resulting in increases in temperature and vapor pressure deficit (VPD) that trigger stomatal closure and hence reduce photosynthesis and NEP indirectly[7]. The stronger positive effect of SM on NEP under drier conditions indicates that the decline in NEP induced by dry SM anomalies cannot be fully offset by increased NEP under wet conditions. Thus, SM variability leads to a net decrease in the mean NEP (Fig. 1a and Fig. S2c). In the tropical and subtropical regions where NEP is strongly limited by SM, SM variations would amplify the interannual variability of NEP (Fig. 1e and Fig. 2a, g).

In contrast to the positive effect of P-E on SM, SM exerts a negative feedback on P-E, particularly in subtropical dry regions (Fig. 2d-f, j-l). Reduced SM strongly limits evapotranspiration but also enhances moisture convergence by regulating atmospheric circulation and vertical ascent[11,12]. The increased moisture convergence partially offsets the decrease in precipitation caused by reduced evapotranspiration, resulting in a negative SM feedback on P-E. While SM changes are largely caused by the P-E dynamics, the negative SM feedback acts to moderate variations in P-E induced by other factors, such as climate warming. This explains the reduced interannual variability in P-E induced by SM variations (Fig. 1f). The SM effect on P-E is pronounced in dry regions/seasons, but rather weak in wet regions/seasons (Fig. 2d-f, j-l), as SM has little impacts on evapotranspiration and moisture convergence under wet conditions[12]. Due to the strong negative feedback associated with dry SM anomalies but not with wet anomalies, SM variability contributes to increased P-E at the global scale, particularly over water-limited regions (Fig. 1b and Fig. S2d).

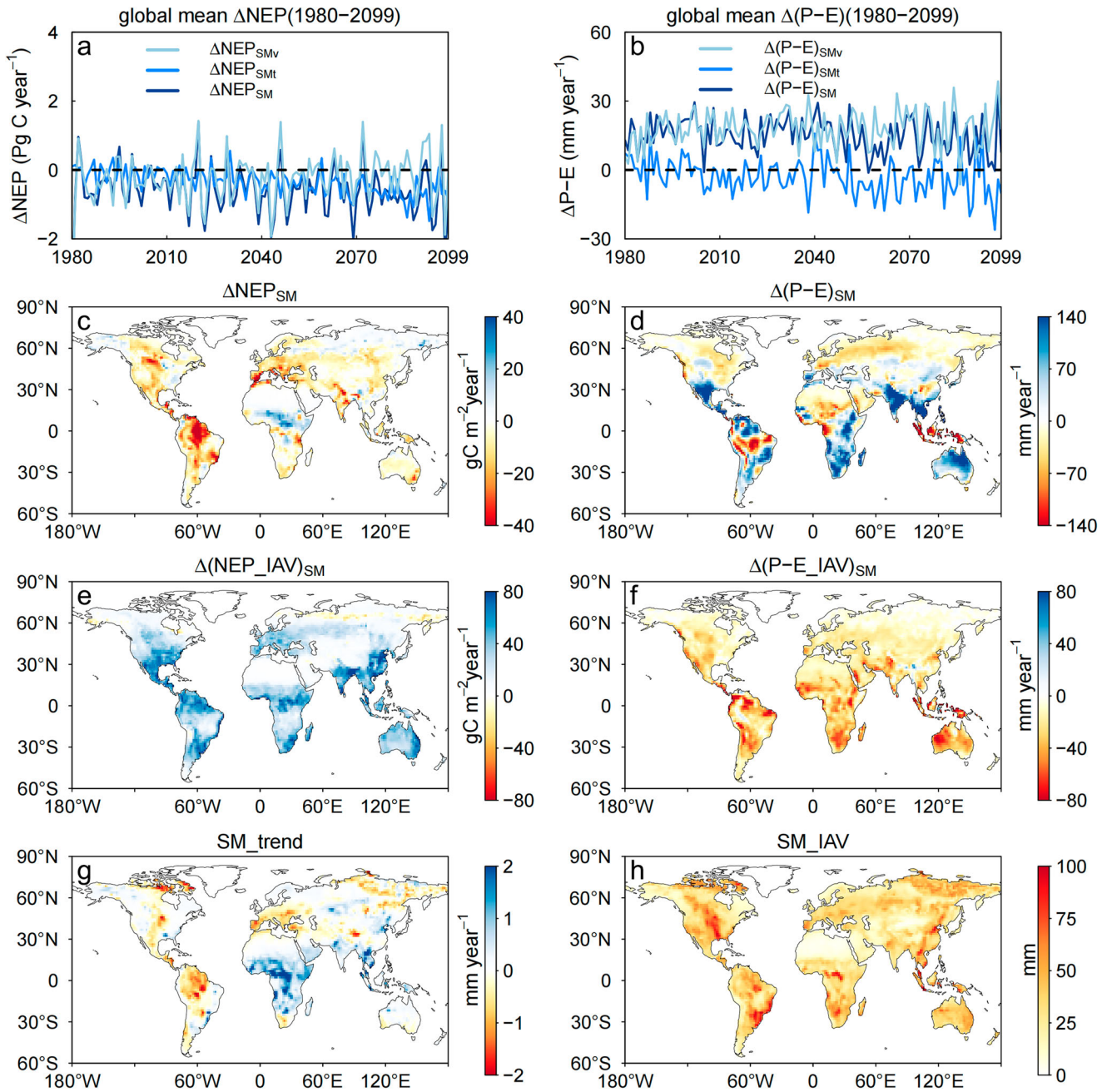

Fig. 1 | SM effects on NEP and P-E during the period of 1980–2099. a,**b** Global area-weighted mean changes in NEP and P-E caused by SM variability (SMv), SM trends (SMt), and total SM changes based on the three ESMs. The total SM effects on the mean (**c**,**d**) and inter-annual variability (IAV, **e**,**f**) of NEP and P-E, which are calculated as their differences in the mean and IAV between coupled simulations (Hist&SSP) and LFMIP experiments (pdLC). In each simulation, the IAV of NEP (or P-E) is quantified as the standard deviation of detrended annual NEP (or P-E), calculated by removing the long-term trend using a 30-year moving average. **g**,**h** Multi-model mean linear trend and IAV of SM in Hist&SSP from 1980 to 2099. The IAV of SM is calculated as the standard deviation of the linearly detrended annual SM.

Carbon-water trade-offs driven by SM–atmosphere interactions

The opposite SM effects on NEP and P-E would contribute to a trade-off between terrestrial carbon uptake and water availability, particularly in the dry season. This is similar to the trade-off between enhanced carbon sink and reduced freshwater supply caused by afforestation and reforestation projects in drylands[28], as forests have access to soil water from deeper and more moist layers and thus increase water expenditure through transpiration and carbon acquisition through photosynthesis concurrently. To test this, we evaluate the Pearson correlation coefficient between SM-induced changes in NEP and P-E, i.e., r(NEP, P-E), which is significantly negative (p-value < 0.05) in all ESMs over more than 90% of assessed land areas, suggesting a widespread trade-off between carbon uptake and water availability driven by SM-atmosphere interactions (Fig. 3a, b). This carbon-water trade-off is further supported by opposing sensitivity coefficients for SM → NEP and SM → (P-E) in the three ESMs (Fig. S5).

The mechanism of the SM-induced carbon-water trade-off is quite different over dry and wet regions (Fig. 3). The carbon (GPP and R) and water (P and E) fluxes controlled by SM dynamics are strongly coupled over many mid-latitude dry regions (Fig. 3c-f). Soil drying limits the exchange of CO_2 and water vapor via plants' stomata, which directly reduces GPP and transpiration, along with reduced soil evaporation (Fig. 3d). In turn, carbon loss via respiration is decreased as GPP drops off, and precipitation

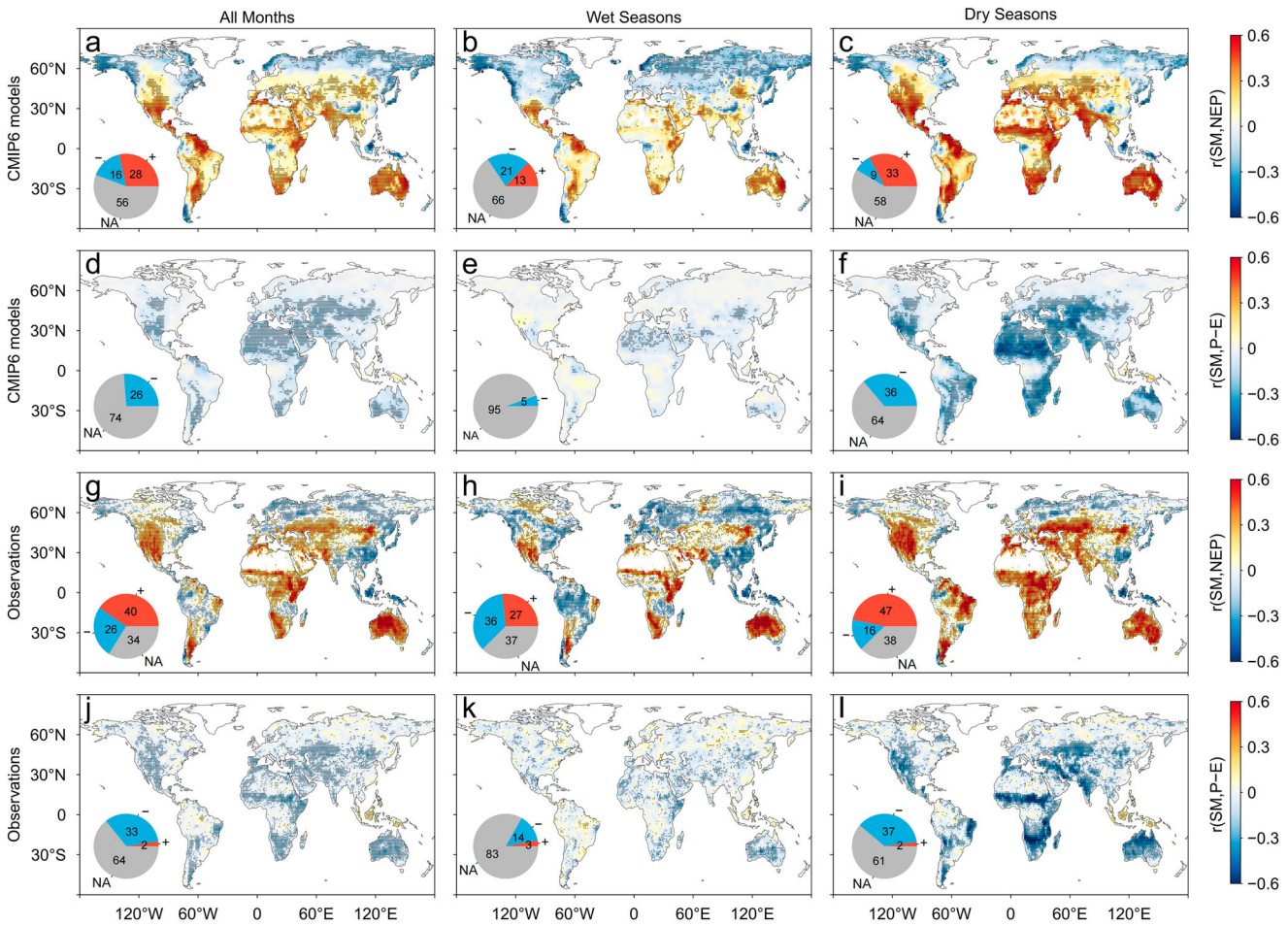

Fig. 2 | Spatial and temporal variations in the SM effects on NEP and P-E in CMIP6 models and observational datasets. a–c Multi-model mean Pearson correlation coefficient, *r*(SM,NEP), between monthly anomalies of SM and NEP from the historical and SSP5-8.5 simulations (1980–2099) for all months (**a**), wet (**b**) and dry (**c**) seasons. **d–f** Multi-model mean Pearson partial correlation coefficient, r (SM,P-E), between anomalies of SM and next month P-E, which isolates the SM feedback on P-E from the direct effect of P-E on SM (see "Methods"). The long-term trends and seasonal cycles of these variables are removed to obtain their monthly anomalies. The dotted areas denote regions where the correlation coefficient is significantly different from zero (p-value < 0.05) and its sign is the same in all ESMs. The pie chart insets show the proportions of land area with significant positive (red) and negative (blue) correlations, and insignificant correlations (gray, labeled as NA). **g–l** The same as (**a**–**f**), but using monthly anomalies of SM, NEP, and P-E from observational datasets.

decreases due to less evaporated water vapor input to the atmosphere. These processes lead to positive relationships between the carbon and water fluxes, particularly the coupling of carbon gain through GPP and water loss via E (Fig. 3c-f). As the direct, positive SM effects on GPP and E are stronger than the indirect effects on R and P, we find a positive SM effect on NEP and a negative effect on P-E that leads to a negative r(NEP, P-E), which is dominated by the strong coupling of GPP and E over mid-latitude dry regions (Fig. 3). A further decomposition of E into transpiration and soil evaporation shows that GPP is strongly coupled with transpiration, while its relationship with soil evaporation is much weaker (Fig. S6). While the SM effects on carbon and water fluxes become much weaker over tropical and extratropical wet regions, the negative *r*(NEP, P-E) is evident and largely caused by the coupling of GPP and E (Fig. 3). The negative *r*(NEP, P-E) also arises from a negative relationship between GPP and P for most wet regions, contrary to their positive relationship over dry regions (Fig. 3c). This is because, when plant photosynthesis is limited by energy availability rather than water supply, increased precipitation, and associated clouds could inhibit photosynthetically active radiation and hence reduce GPP in wet regions[41].

In addition to the dry season, the SM-induced carbon-water trade-off persists during the wet season, although it weakens across many regions (Fig. S7a, b). The negative *r*(NEP, P-E) remains due to the stronger negative relationship between P and NEP (GPP-R), despite the reduced coupling between GPP and E (Fig. S7). The global prevalence of SM-induced trade-off between carbon and water exchanges in both dry and wet seasons as shown in Figs. 3 and S7 reinforces the importance of SM dynamics in regulating coupled carbon and water cycling.

SM-induced intensification of carbon-water trade-offs in the future

Figures 1a, b and S3 show that the SM effects on NEP and P-E are increasing over time at the global scale, irrespective of whether SM increases or decreases from 1980 to 2099. To further examine this, we compare the 30-year historical (1980–2009) and future (2070–2099, SSP5-8.5) periods. While the global patterns of SM effects on the mean NEP and P-E are similar between the two periods, the magnitudes of positive and negative SM effects are amplified by increased SM variability and the SM drying trend (Figs. 4 and S8). We also note the wetting of SM increases NEP and decreases P-E and offsets the effect of SM variability, such as in North Africa (Fig. 4c, f). In addition to the mean, the SM effects on the interannual variability of NEP and P-E are also projected to be stronger in the future (Fig. 4g-l). Increased SM variability due to climate change further increases the variability of NEP and reduces the variability of P-E over most land areas (Fig. 4i, l and Fig. S8b).

Amplification of the opposite SM impacts on NEP and P-E would lead to a stronger trade-off between terrestrial carbon uptake and water

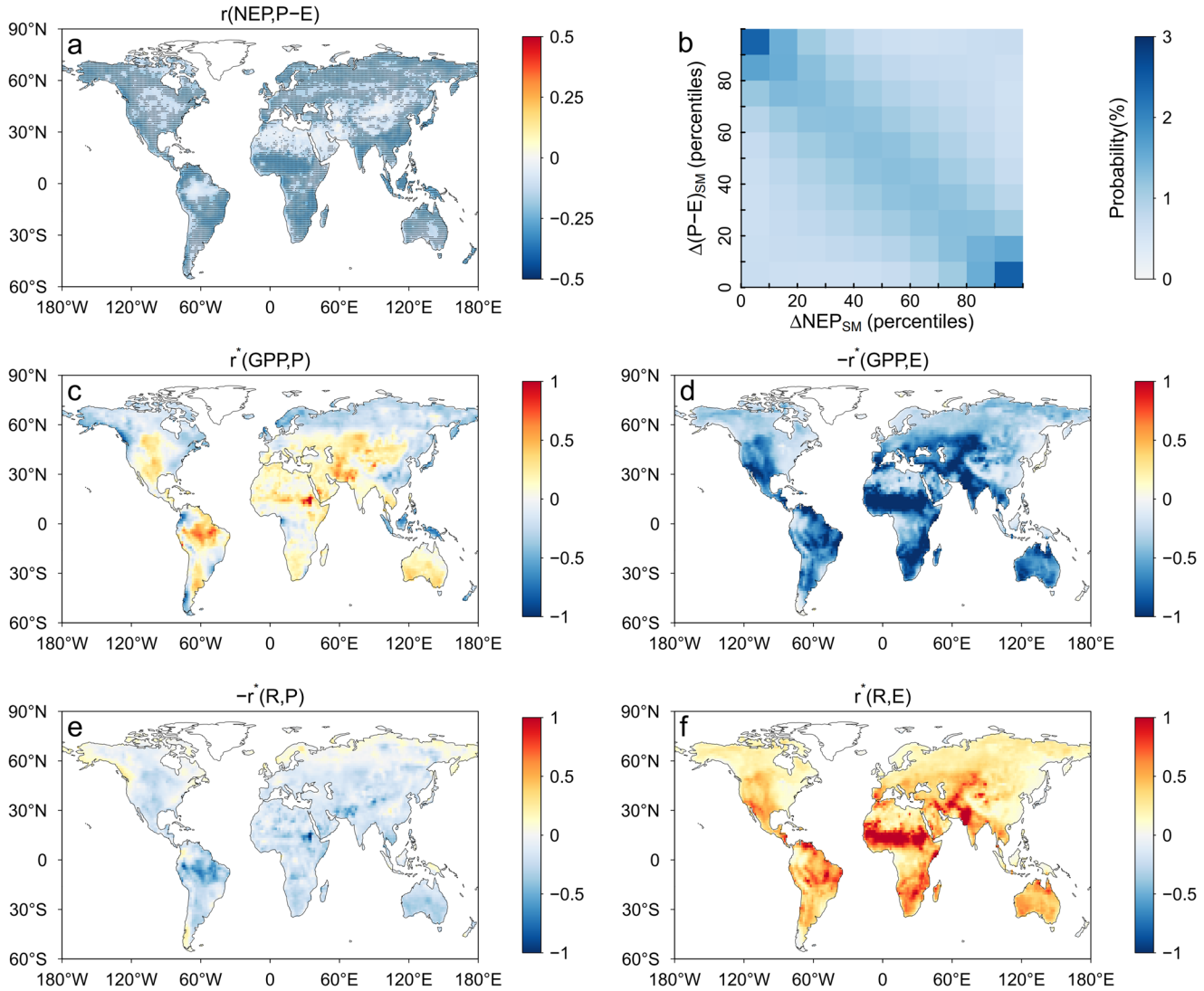

Fig. 3 | SM-induced trade-off between NEP and P-E in dry seasons during the period of 1980-2099. a Multi-model mean Pearson correlation coefficient, *r*(NEP, P-E), between SM-induced changes in NEP (ΔNEP_{SM}) and P-E ($\Delta(P\text{-}E)_{SM}$), which are calculated as the their differences between coupled simulations (Hist&SSP) and LFMIP experiments (pdLC). The dotted areas denote regions where r(NEP, P-E) is significantly different from zero (*p*-value < 0.05) and its sign is the same in all ESMs. **b** Trade-off between ΔNEP_{SM} and $\Delta(P\text{-}E)_{SM}$ in terms of the mean probability for each decile of ΔNEP_{SM} and $\Delta(P\text{-}E)_{SM}$ across land grid cells. **c–f** Decomposed contributions to *r*(NEP, P-E) from the coupling (r^*) of SM-induced changes in carbon (GPP and R) and water (P and E) fluxes (see Methods).

availability in the future. Indeed, the negative correlation between NEP and P-E induced by SM variations is projected to be amplified in the future (Fig. S9). As carbon and water fluxes are more sensitive to SM under drier conditions (Fig. 2), the projected SM drying leads to enhanced water controls on photosynthetic carbon uptake and evaporative water loss, resulting in a tighter coupling of GPP and E and hence a stronger trade-off between NEP and P-E in water-limited regions (Figs. S8 and S9). This reflects the increasing importance of SM changes in the coupled carbon and water cycling over terrestrial ecosystems in the future.

Discussion

Understanding the responses of coupled water and carbon cycles to global environmental changes is crucial for achieving mitigation and adaptation to climate change. Earlier studies have mostly highlighted rising temperature and elevated CO_2 as dominant environmental drivers in global carbon and water cycling[42–45]. While the large influences of SM on carbon uptake and water availability have been reported in recent years[7,9,11,12,46], the potential SM regulation of the carbon-water coupling has not been well recognized. Our modeling and observational evidence demonstrate a pronounced trade-off due to the opposite effects of SM on the mean and interannual variability of terrestrial carbon uptake and water availability around the globe. The trade-off between NEP and P-E and its amplification in a warming and drying future are dominated by the strong coupling of carbon gain via GPP and water loss through E over vegetated areas. This suggests that the SM impacts on the coupled carbon and water cycling mainly depend on how vegetation responds to water stress, and increasing ecosystem water use efficiency (GPP/E) is therefore crucial to enhancing land carbon sink and alleviating the cost of reduced freshwater availability in the future.

The SM-induced trade-offs between carbon uptake and water availability have important implications for sustainable management of ecosystem services, such as the provision of water, food and wood, and maintenance of carbon stocks and biodiversity[31,47,48]. Considering that the impacts of SM and vegetation on carbon uptake and water availability are strongly coupled within the soil-plant-atmosphere continuum[32,33], the identified trade-off pattern in Fig. 3 could inform future restoration projects to determine priority areas for afforestation and reforestation, which have been promoted as nature-based solutions for CO_2 removal and climate change mitigation[34,49]. However, many forest restoration programs have overlooked the potential consequences on freshwater availability, leading to

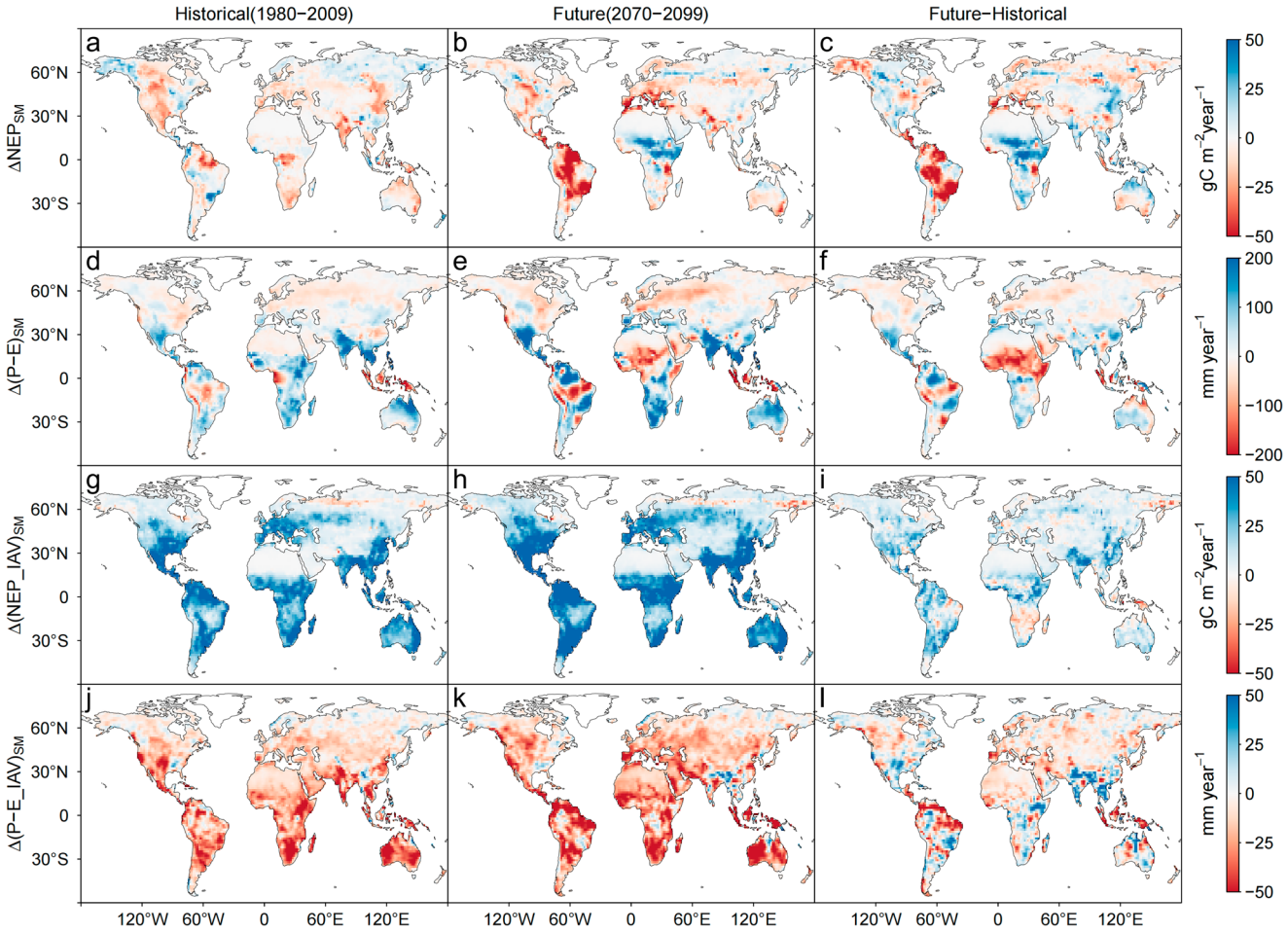

Fig. 4 | Changes in the SM effects on the mean and variability of NEP and P-E between the historical and future periods. a–f Multi-model mean SM effects on NEP and P-E, which are calculated as the differences in NEP and P-E between the coupled simulations (Hist&SSP) and LFMIP experiments (pdLC), during the historical (1980–2009) and future (2070-2099, SSP5-8.5) periods based on the ESMs. **g–l** The same as (**a**–**f**), but for the SM effects on the inter-annual variability (IAV) of NEP and P-E, which are calculated as the differences in the standard deviation of detrended NEP and P-E between Hist&SSP and pdLC.

increased forestation at the expense of local water resources, for example over drylands[28,31,50], where the carbon-water trade-off is significant (Fig. 3) and may become stronger when excessive water consumption by increased vegetation cover accelerates the decline in SM. By comparison, forest restoration and conservation might be more effective in tropical regions where the trade-off is less pronounced and the potential for carbon storage is the greatest[51], offering optimal conditions to achieve the co-benefits of carbon gain and water sustainability. In addition, the carbon-water trade-off driven by SM-atmosphere interactions will be further enhanced by amplified SM controls on carbon uptake and water availability under future climate change, which may reduce the carbon storage potential by taking into account the sustainability of water resources. This presents a major challenge to realizing a number of sustainable development goals related to carbon uptake and water availability at the same time.

The identified SM effects on the coupled carbon and water cycling based on the LFMIP experiments include both direct effects of soil water limitation on evapotranspiration and carbon uptake, and indirect effects via SM-induced changes in precipitation, temperature, and VPD[7,11]. The negative SM feedback on P-E mitigates the decrease in P-E and may alleviate SM drying by enhancing moisture influx[11,12]. In contrast, the positive SM feedback on VPD strongly accelerates regional SM drying and amplifies the reduction in NEP[7,24]. Together, these two distinct feedback pathways contribute to the carbon-water trade-off induced by SM variations. While the positive effect of SM on NEP and the negative effect on P-E, as well as their trade-off relationship, are evident in the ESMs, the sign and magnitude of the net SM effects on these carbon and water fluxes vary across models (Figs. S3 and S5). These variations may arise from uncertainties in simulated SM changes and inaccurate representations of vegetation responses to SM dynamics and land-atmosphere interactions. In particular, the vegetation water stress processes related to stomatal, xylem, and root traits, which show biases compared with observations[13,52], and the underestimated strength of land-atmosphere coupling[53], might have introduced substantial uncertainties in the identified SM effects on P-E and NEP, thereby limiting the accuracy of our analyses. Additionally, the SM effects on carbon and water fluxes might be overestimated due to the use of the extreme high-emission scenario. Improved simulations of SM variations under more realistic forcing scenarios, coupled with enhanced representations of soil-vegetation-atmosphere interactions, would potentially reduce uncertainties in both current and future projections of terrestrial carbon and water fluxes.

Our findings underscore the importance of soil moisture in regulating the coupled carbon and water cycling in terrestrial ecosystems. While our mechanistic understanding of the soil moisture effects on the coupling of carbon and water fluxes relies mostly on Earth system model experiments, it has broader implications for predicting changes in terrestrial carbon and water cycling in the real world, such as the observed trade-off between carbon sink and water resources induced by human activities such as irrigation and afforestation[28,54]. Given the extensive influence of SM on the Earth system, additional trade-offs could be identified by evaluating the simultaneous impacts of SM changes on various processes, such as increased drought and flood risks, soil erosion,

soil degradation, water quality deterioration, vegetation dynamics, and crop yield reductions. These broader trade-offs underscore the importance of a more nuanced understanding of the positive and negative consequences of SM changes across climatic, ecological, hydrological, and agricultural systems. Moreover, an improved understanding of the coupled carbon and water cycling and particular the roles of land surface characteristics, such as soil moisture and vegetation cover, based on observations and model simulations will guide land management practices (e.g., land use transformation, forest restoration) to optimize multiple ecosystem services, such as carbon, food, and water, and support policy-making to better manage terrestrial ecosystems for climate change mitigation and adaptation in the future[30,31,55,56].

Methods

CMIP6 and LFMIP simulations

We used the historical (1980–2014) and the shared Socioeconomic Pathway 5-8.5 (SSP5-8.5, 2015–2099) simulations (collectively termed Hist&SSP) in CMIP6 and corresponding simulations driven by the same forcings (e.g., greenhouse gases, land use, sea surface temperatures, and sea ice) as those from Hist&SSP in the Land Feedback Model Intercomparison Project (LFMIP)[35]. We used the extreme high-emission scenario (SSP5-8.5) because moderate forcing scenarios have not yet been adopted by LFMIP. Three Earth System Models (CMCC-ESM2, IPSL-CM6A-LR, MPI-ESM1-2-LR) that participated in the LFMIP experiments were selected for this study. These ESMs incorporate our current understanding of global water and carbon cycles and their interactions while meeting the data requirements for our analysis. The other climate models in LFMIP, which do not represent the carbon cycle and/or dynamic responses of vegetation cover and physiology (i.e., carbon and water exchanges through stomata) to elevated CO_2 concentrations and climate change, were excluded. For each ESM, we used two simulations in LFMIP: amip-lfmip-pdLC (pdLC) and amip-lfmip-rmLC (rmLC). These simulations differ from corresponding Hist&SSP only in terms of the SM settings. SM was fully coupled with the atmosphere in Hist&SSP, while it was prescribed as the 1980–2014 climatology (pdLC) and a transient 30-year running mean climatology (rmLC) from Hist&SSP throughout the LFMIP simulation period of 1980–2099 (see Fig. S1 for an example).

The LFMIP experiment builds on the Global Land Atmosphere Coupling Experiment (GLACE)-CMIP5, aiming to assess the SM-atmosphere coupling and associated impacts on weather and climate in CMIP6[57,58]. These experiments have also been used to evaluate the SM effects on global carbon and water cycling[9–12]. By comparing the fully coupled Hist&SSP and the SM-prescribed pdLC and rmLC, the SM effects on P-E and NEP can be isolated (see the section "SM effects on NEP and P-E in model simulations"). This includes the direct effects of soil water stress on evapotranspiration, photosynthesis, and respiration, as well as the indirect effects arising from changes in air temperature, humidity, and precipitation induced by SM-atmosphere feedbacks[10,12]. For our analyses, we used monthly total soil moisture content ("mrso"), precipitation ("pr"), evapotranspiration ("evspsbl"), net ecosystem production ("nep"), and gross primary production ("gpp") from the three ESMs. In addition, precipitation-minus-evapotranspiration (P-E) and ecosystem respiration (R), i.e., the difference between GPP and NEP, were also computed in each model. We also used transpiration ("tran"), which is available only in IPSL-CM6A-LR and MPI-ESM1-2-LR. Soil evaporation was derived by taking away transpiration from evapotranspiration.

Observation-based datasets

To identify the SM effects on NEP and P-E, we also used monthly root-zone soil moisture (0–100 cm), total precipitation, and evapotranspiration from the European Centre for Medium-Range Weather Forecasts (ERA5)[37] and monthly outputs of net ecosystem exchange from the FLUXCOM dataset[38] during the period of 1979–2018. The ERA5 global reanalysis was constrained by a large number of in situ and satellite remote sensing observations and can well represent the relationship between SM and P-E[11,12]. The FLUXCOM dataset was produced by upscaling carbon flux measurements from 224 eddy covariance towers using three machine learning methods and satellite remote sensing and meteorological/climate forcings. We used the FLUXCOM ensemble-driven by remote sensing and the ERA5 climate forcing. Using these observation-based datasets, we were able to assess the seasonally varying SM effects on NEP and P-E based on correlation analysis and compare the results with model simulations (see the section "SM effects on NEP and P-E based on correlation analysis").

SM effects on NEP and P-E in model simulations

To isolate the SM effects on carbon and water fluxes, we used the historical and SSP5-8.5 simulations (Hist&SSP) and the two LFMIP simulations (pdLC and rmLC) with prescribed SM during 1980–2099. Comparing the carbon and water fluxes in the three simulations, we were able to isolate the total effect of SM (Hist&SSP-pdLC) as well as the effects of SM trends (rmLC-pdLC) and variability (Hist&SSP-rmLC).

We used monthly data from the three simulations above in each model to assess the long-term SM effects on NEP and P-E. For example, we isolated the effect of SM on NEP as follows:

$$\Delta NEP_{SM} = NEP_{hs} - NEP_{pd} \quad (1)$$

where ΔNEP_{SM} is the change in NEP caused by SM changes, NEP_{hs} and NEP_{pd} represent the NEP in Hist&SSP and pdLC, respectively. ΔNEP_{SM} can be further separated into the contributions of SM variability (ΔNEP_{SMv}) and SM trends (ΔNEP_{SMt}):

$$\Delta NEP_{SM} = \Delta NEP_{SMv} + \Delta NEP_{SMt} \quad (2)$$

ΔNEP_{SMv} and ΔNEP_{SMt} are calculated as the difference in NEP between Hist&SSP and rmLC and between rmLC and pdLC, respectively. The SM effects on P-E can be isolated in a similar way:

$$\Delta(P-E)_{SM} = (P-E)_{hs} - (P-E)_{pd} \quad (3)$$

$$\Delta(P-E)_{SM} = \Delta(P-E)_{SMv} + \Delta(P-E)_{SMt} \quad (4)$$

We first assessed the effects of total SM changes as well as their trends and variability on NEP and P-E during 1980–2099 (120 years in total) at the global scale. Further, we identified the global patterns of SM effects on the long-term mean and interannual variability of NEP and P-E during the study period. We also examined whether the SM effects on NEP and P-E would be amplified or attenuated in the future by comparing the historical (1980–2009) and future (2070–2099) periods. Model results were bilinearly interpolated to a spatial resolution of 1.5° × 1.5° to obtain the multi-model mean results in our analyses. R (version 4.2.2) was used for data analysis and producing all the figures for this study.

SM effects on NEP and P-E based on correlation analysis

In addition to the comparison of Hist&SSP and LFMIP simulations above, we identified the direction and magnitude of SM effects on NEP and P-E based on a correlation analysis using model outputs from Hist&SSP (1980-2099) and observation-based datasets (1979–2018). We used the Pearson correlation coefficient, which measures the direction and strength of the linear relationship between two variables, to show how strongly the carbon and water fluxes respond to SM variations[13]. As NEP is unidirectionally controlled by SM at the ecosystem scale[7,9], we calculated the correlation coefficient between anomalies of SM and NEP to characterize the SM effect on NEP, with the long-term trends and seasonal cycles of these variables (i.e., 30-year running mean monthly values) removed to reduce the potential influence of other factors.

To identify the SM effect on P-E, we assessed the relationship between anomalies of monthly SM and the P-E in the following month. This is because P-E and SM are strongly coupled, and the relatively weak SM

feedback on P-E may be masked by the direct, positive impact of P-E on SM[11,12]. The causal relationship between SM and P-E could be identified based on temporally lagged correlation, which has been widely used to assess the SM-atmosphere feedbacks[59–61]. As the P-E effect on SM may persist for weeks to months due to the relatively long SM memory arising from slow processes of soil water percolation and evaporation[62], the one-month lagged correlation between SM and P-E may also reflect the autocorrelation of P-E[11,12,60]. To remove the potential effect of P-E autocorrelation, we used the Pearson partial correlation coefficient between anomalies of SM and next month P-E given current month P-E to isolate the SM effect on P-E from the direct impact of P-E on SM.

As the SM effects on carbon and water fluxes may vary seasonally[9,12], we further applied the correlation analysis to identify the SM effects on NEP and P-E for wet and dry seasons, which were defined as the highest and lowest consecutive six months of P-E, respectively. Given that SM is higher in the wet season and lower in the dry season, this also allows us to identify the non-linear relationship between SM and NEP or P-E, as well as the impacts of SM variability on NEP and P-E. To better characterize the non-linear relationship between SM and carbon/water fluxes, we also used the Spearman (partial) correlation coefficient, which does not assume linearity and measures the direction and strength of the monotonic relationship between two variables. The correlation results from the two kinds of correlation coefficients are highly consistent (Figs. 2 and S4), demonstrating robust effects of SM on carbon and water fluxes.

SM-induced trade-off between NEP and P-E

To quantify the trade-off of SM impacts on carbon uptake and water availability, we assessed the Pearson correlation coefficient, i.e., $r(NEP, P-E)$, between SM-induced changes in NEP (ΔNEP_{SM}) and P-E ($\Delta(P-E)_{SM}$) in the dry season. The trade-off between ΔNEP_{SM} and $\Delta(P-E)_{SM}$ could be attributed to the coupling of carbon (GPP and R) and water (P and E) fluxes induced by SM variations. To do so, we decomposed $r(NEP, P-E)$ into four components as follows:

$$r(NEP, P-E) = \frac{cov(GPP-R, P-E)}{\sigma_{NEP} \cdot \sigma_{P-E}} \quad (5)$$

or

$$r(NEP, P-E) = \frac{cov(GPP, P)}{\sigma_{NEP} \cdot \sigma_{P-E}} - \frac{cov(GPP, E)}{\sigma_{NEP} \cdot \sigma_{P-E}} - \frac{cov(R, P)}{\sigma_{NEP} \cdot \sigma_{P-E}} + \frac{cov(R, E)}{\sigma_{NEP} \cdot \sigma_{P-E}} \quad (6)$$

where σ_{NEP} and σ_{P-E} represent the standard deviations of ΔNEP_{SM} and $\Delta(P-E)_{SM}$, respectively, in the dry season, and $\mathrm{cov}(C, W)$ is the covariance between SM-induced changes in carbon (ΔC_{SM}, i.e., ΔGPP_{SM} and ΔR_{SM}) and water (ΔW_{SM}, i.e., ΔP_{SM} and ΔE_{SM}) fluxes. ΔC_{SM} and ΔW_{SM} can be calculated in a similar fashion as Eqs. (1) and (3). The four components represent the contributions of the coupling between each pair of carbon and water fluxes on the right-hand side of Eq. (6), which can be re-organized as:

$$\begin{aligned} r(NEP, P-E) = {} & r(GPP, P)\frac{\sigma_{GPP} \cdot \sigma_P}{\sigma_{NEP} \cdot \sigma_{P-E}} - r(GPP, E)\frac{\sigma_{GPP} \cdot \sigma_E}{\sigma_{NEP} \cdot \sigma_{P-E}} \\ & - r(R, P)\frac{\sigma_R \cdot \sigma_P}{\sigma_{NEP} \cdot \sigma_{P-E}} + r(R, E)\frac{\sigma_R \cdot \sigma_E}{\sigma_{NEP} \cdot \sigma_{P-E}} \end{aligned} \quad (7)$$

or

$$r(NEP, P-E) = r^*(GPP, P) - r^*(GPP, E) - r^*(R, P) + r^*(R, E) \quad (8)$$

where $r(C, W)\frac{\sigma_C \cdot \sigma_W}{\sigma_{NEP} \cdot \sigma_{P-E}}$ is simplified as $r^*(C, W)$ and represents the contribution of the coupling between ΔC_{SM} and ΔW_{SM} to $r(NEP, P-E)$. Similarly, $-r^*(GPP, E)$ is decomposed into the contributions of transpiration ($-r^*(GPP, T)$) and soil evaporation ($-r^*\left(GPP, E_s\right)$).

Reporting summary

Further information on research design is available in the Nature Portfolio Reporting Summary linked to this article.

Data availability

The CMIP6 model simulations (including LFMIP simulations) are publicly available from https://esgf-node.llnl.gov/search/cmip6/. The ERA5 dataset is available from https://cds.climate.copernicus.eu/cdsapp#!/dataset/reanalysis-era5-single-levels-monthly-means?tab=overview and the FLUXCOM dataset from https://www.bgc-jena.mpg.de/geodb/projects/Home.php.

Code availability

The R code used for data analyses is available upon request.

Received: 14 October 2024; Accepted: 18 February 2025;
Published online: 01 March 2025

References

1. Friedlingstein, P. et al. Global Carbon Budget 2021. *Earth Syst. Sci. Data* **14**, 1917–2005 (2022).
2. Zhou, S., Yu, B., Lintner, B. R., Findell, K. L. & Zhang, Y. Projected increase in global runoff dominated by land surface changes. *Nat. Clim. Chang.* **13**, 442–449 (2023).
3. Gu, B., Zhou, S., Yu, B., Findell, K. L. & Lintner, B. R. Multifaceted changes in water availability with a warmer climate. *npj Clim. Atmos. Sci.* **8**, 31 (2025).
4. Piao, S. et al. The impacts of climate extremes on the terrestrial carbon cycle: a review. *Sci. China Earth Sci.* **62**, 1551–1563 (2019).
5. Reichstein, M. et al. Climate extremes and the carbon cycle. *Nature* **500**, 287–295 (2013).
6. Zhang, S. et al. Reconciling disagreement on global river flood changes in a warming climate. *Nat. Clim. Chang.* **12**, 1160–1167 (2022).
7. Humphrey, V. et al. Soil moisture–atmosphere feedback dominates land carbon uptake variability. *Nature* **592**, 65–69 (2021).
8. Zhou, S. et al. Large divergence in tropical hydrological projections caused by model spread in vegetation responses to elevated CO2. *Earth's Future* **10**, e2021EF002457 (2022).
9. Green, J. K. et al. Large influence of soil moisture on long-term terrestrial carbon uptake. *Nature* **565**, 476 (2019).
10. Humphrey, V. et al. Sensitivity of atmospheric CO2 growth rate to observed changes in terrestrial water storage. *Nature* **560**, 628–631 (2018).
11. Zhou, S. et al. Soil moisture–atmosphere feedbacks mitigate declining water availability in drylands. *Nat. Clim. Chang.* **11**, 38–44 (2021).
12. Zhou, S. et al. Diminishing seasonality of subtropical water availability in a warmer world dominated by soil moisture–atmosphere feedbacks. *Nat. Commun.* **13**, 5756 (2022).
13. Kannenberg, S. A., Anderegg, W. R. L., Barnes, M. L., Dannenberg, M. P. & Knapp, A. K. Dominant role of soil moisture in mediating carbon and water fluxes in dryland ecosystems. Nat. Geosci. https://doi.org/10.1038/s41561-023-01351-8 (2024).
14. Song, J. et al. Serious underestimation of reduced carbon uptake due to vegetation compound droughts. *npj Clim. Atmos. Sci.* **7**, 23 (2024).
15. Berg, A., Sheffield, J. & Milly, P. C. D. Divergent surface and total soil moisture projections under global warming. *Geophys. Res. Lett.* **44**, 236–244 (2017).
16. Fuso Nerini, F. et al. Connecting climate action with other Sustainable Development Goals. *Nat. Sustain.* **2**, 674–680 (2019).
17. Nilsson, M., Griggs, D. & Visbeck, M. Map the interactions between Sustainable Development Goals. *Nature* **534**, 320–322 (2016).
18. Fu, Z. et al. Critical soil moisture thresholds of plant water stress in terrestrial ecosystems. *Sci. Adv.* **8**, eabq7827 (2022).

19. Liu, L. et al. Soil moisture dominates dryness stress on ecosystem production globally. *Nat. Commun.* **11**, 4892 (2020).
20. Gentine, P. et al. Coupling between the terrestrial carbon and water cycles—a review. *Environ. Res. Lett.* **14**, 083003 (2019).
21. Nie, C. et al. Effects of soil water content on forest ecosystem water use efficiency through changes in transpiration/evapotranspiration ratio. *Agric. For. Meteorol.* **308–309**, 108605 (2021).
22. Boese, S., Jung, M., Carvalhais, N., Teuling, A. J. & Reichstein, M. Carbon–water flux coupling under progressive drought. *Biogeosciences* **16**, 2557–2572 (2019).
23. Zhou, S., Zhang, Y., Williams, A. P. & Gentine, P. Projected increases in intensity, frequency, and terrestrial carbon costs of compound drought and aridity events. *Sci. Adv.* **5**, eaau5740 (2019).
24. Zhou, S. et al. Land–atmosphere feedbacks exacerbate concurrent soil drought and atmospheric aridity. *PNAS* **116**, 18848–18853 (2019).
25. Guillod, B. P., Orlowsky, B., Miralles, D. G., Teuling, A. J. & Seneviratne, S. I. Reconciling spatial and temporal soil moisture effects on afternoon rainfall. *Nat. Commun.* **6**, 6443 (2015).
26. Koster, R. D. et al. Regions of strong coupling between soil moisture and precipitation. *Science* **305**, 1138–1140 (2004).
27. May, W., Rummukainen, M., Chéruy, F., Hagemann, S. & Meier, A. Contributions of soil moisture interactions to future precipitation changes in the GLACE-CMIP5 experiment. *Clim. Dyn.* **49**, 1681–1704 (2017).
28. Feng, X. et al. Revegetation in China's Loess Plateau is approaching sustainable water resource limits. *Nat. Clim. Change* **6**, 1019–1022 (2016).
29. Lan, X., Liu, Z., Chen, X., Lin, K. & Cheng, L. Trade-off between carbon sequestration and water loss for vegetation greening in China. *Agric. Ecosyst. Environ.* **319**, 107522 (2021).
30. Bayer, A. D., Lautenbach, S. & Arneth, A. Benefits and trade-offs of optimizing global land use for food, water, and carbon. *Proc. Natl. Acad. Sci. USA***120**, e2220371120 (2023).
31. Li, R. et al. Time and space catch up with restoration programs that ignore ecosystem service trade-offs. *Sci. Adv.* **7**, eabf8650 (2021).
32. Li, Z. et al. A comprehensive review on coupled processes and mechanisms of soil-vegetation-hydrology, and recent research advances. *Sci. China Earth Sci.* **65**, 2083–2114 (2022).
33. Silva, L. C. R. & Lambers, H. Soil-plant-atmosphere interactions: structure, function, and predictive scaling for climate change mitigation. *Plant Soil* **461**, 5–27 (2021).
34. Jung, M. et al. Areas of global importance for conserving terrestrial biodiversity, carbon and water. *Nat. Ecol. Evol.* **5**, 1499–1509 (2021).
35. van den Hurk, B. et al. LS3MIP (v1.0) contribution to CMIP6: the Land Surface, Snow and Soilmoisture Model Intercomparison Project—aims, setup and expected outcome. *Geosci. Model Dev.* **9**, 2809–2832 (2016).
36. Eyring, V. et al. Overview of the Coupled Model Intercomparison Project Phase 6 (CMIP6) experimental design and organization. *Geosci. Model Dev.* **9**, 1937–1958 (2016).
37. Hersbach, H. et al. The ERA5 global reanalysis. *Q. J. R. Meteorol. Soc.* **146**, 1999–2049 (2020).
38. Jung, M. et al. Scaling carbon fluxes from eddy covariance sites to globe: synthesis and evaluation of the FLUXCOM approach. *Biogeosciences* **17**, 1343–1365 (2020).
39. Ahlström, A. et al. The dominant role of semi-arid ecosystems in the trend and variability of the land CO 2 sink. *Science* **348**, 895–899 (2015).
40. Poulter, B. et al. Contribution of semi-arid ecosystems to interannual variability of the global carbon cycle. *Nature* **509**, 600–603 (2014).
41. Wei, S. et al. Prolonged impacts of extreme precipitation events weakened annual ecosystem CO2 sink strength in a coastal wetland. *Agric. For. Meteorol.* **310**, 108655 (2021).
42. Cheng, L. et al. Recent increases in terrestrial carbon uptake at little cost to the water cycle. *Nat. Commun.* **8**, 110 (2017).
43. Schimel, D., Stephens, B. B. & Fisher, J. B. Effect of increasing CO2 on the terrestrial carbon cycle. *Proc. Natl. Acad. Sci. USA***112**, 436–441 (2015).
44. Wang, X. et al. A two-fold increase of carbon cycle sensitivity to tropical temperature variations. *Nature* **506**, 212–215 (2014).
45. Zhou, S. et al. Response of water use efficiency to global environmental change based on output from terrestrial biosphere models: drivers of WUE variability. *Glob. Biogeochem. Cycles* **31**, 1639–1655 (2017).
46. Liu, L. et al. Increasingly negative tropical water–interannual CO2 growth rate coupling. *Nature* **618**, 755–760 (2023).
47. Chisholm, R. A. Trade-offs between ecosystem services: Water and carbon in a biodiversity hotspot. *Ecol. Econ.* **69**, 1973–1987 (2010).
48. Kim, J. H., Jobbágy, E. G. & Jackson, R. B. Trade-offs in water and carbon ecosystem services with land-use changes in grasslands. *Ecol. Appl.* **26**, 1633–1644 (2016).
49. Griscom, B. W. et al. Natural climate solutions. *Proc. Natl. Acad. Sci. USA***114**, 11645–11650 (2017).
50. Cui, J. et al. Global water availability boosted by vegetation-driven changes in atmospheric moisture transport. *Nat. Geosci*. https://doi.org/10.1038/s41561-022-01061-7 (2022).
51. Mo, L. et al. Integrated global assessment of the natural forest carbon potential. *Nature* **624**, 92–101 (2023).
52. Zhao, M., A, G., Liu, Y. & Konings, A. G. Evapotranspiration frequently increases during droughts. *Nat. Clim. Chang*. https://doi.org/10.1038/s41558-022-01505-3 (2022).
53. Green, J. K. et al. Regionally strong feedbacks between the atmosphere and terrestrial biosphere. *Nat. Geosci.* **10**, 410–414 (2017).
54. Xi, Y. et al. Trade-off between tree planting and wetland conservation in China. *Nat. Commun.* **13**, 1967 (2022).
55. Ma, S., Zhou, S., Yu, B. & Song, J. Deforestation-induced runoff changes dominated by forest-climate feedbacks. *Sci. Adv.* **10**, eadp3964 (2024).
56. Xu, H., Yue, C., Zhang, Y., Liu, D. & Piao, S. Forestation at the right time with the right species can generate persistent carbon benefits in China. *Proc. Natl. Acad. Sci. USA***120**, e2304988120 (2023).
57. Qiao, L. et al. Soil moisture–atmosphere coupling accelerates global warming. *Nat. Commun.* **14**, 4908 (2023).
58. Seneviratne, S. I. et al. Impact of soil moisture-climate feedbacks on CMIP5 projections: First results from the GLACE-CMIP5 experiment. *Geophys. Res. Lett.* **40**, 5212–5217 (2013).
59. D'Odorico, P. & Porporato, A. Preferential states in soil moisture and climate dynamics. *Proc. Natl. Acad. Sci.* **101**, 8848–8851 (2004).
60. Wei, J., Dickinson, R. E. & Chen, H. A negative soil moisture–precipitation relationship and its causes. *J. Hydrometeor.* **9**, 1364–1376 (2008).
61. Zhang, J., Wang, W.-C. & Wei, J. Assessing land-atmosphere coupling using soil moisture from the Global Land Data Assimilation System and observational precipitation. *J. Geophys. Res. Atmos.* **113**, (2008).
62. Seneviratne, S. I. et al. Soil moisture memory in AGCM simulations: analysis of Global Land–Atmosphere Coupling Experiment (GLACE) data. *J. Hydrometeor.* **7**, 1090–1112 (2006).

Acknowledgements

We acknowledge the World Climate Research Programme's Working Group on Coupled Modelling, which is responsible for CMIP, and we thank the climate modeling groups for producing and making available their model output. For CMIP the U.S. Department of Energy's Program for Climate Model Diagnosis and Intercomparison provides coordinating support and led development of software infrastructure in partnership with the Global Organization for Earth System Science Portals. This work was supported by the National Key Research and Development Program of China (2022YFF0801303), the NSFC Excellent Young Scientists Fund (Overseas), and the Fundamental Research Funds for the Central Universities.

Author contributions

S.Z. conceived and designed the study. W.S. and S.Z. performed the observational and modeling data analyses. S.Z. and W.S. wrote the manuscript. B.Y., Y.Z., T.K., and B.F. commented on the results and edited the manuscript.

Competing interests

The authors declare no competing interests.

Additional information

Supplementary information The online version contains supplementary material available at https://doi.org/10.1038/s43247-025-02145-z.

Correspondence and requests for materials should be addressed to Sha Zhou.

Peer review information *Communications Earth & Environment* thanks the anonymous reviewers for their contribution to the peer review of this work. Primary Handling Editor: Alireza Bahadori. A peer review file is available.